The Iranian Journal of Mechanical Engineering Transactions of ISME
Journal homepage: https://jmee.isme.ir
Vol. 24, No. 1, 2023, pp. 70-84

Research Paper

DOI: https://doi.org/10.30506/jmee.2023.1982755.1307
DOR: https://dorl.net/dor/20.1001.1.16059727.2023.24.1.5.9

Multi-objective Optimization of Two-Layer Microbeam used for Sensing of Viruses by Genetic Algorithm

Mohammadreza Davoodi Yekta[*]
M.Sc.

Abbas Rahi[†]
Assistant Professor

In this paper, new optimizations of the two-layer microbeams based on the classical and non-classical theory are presented. In the first step, the natural frequency is obtained based on the modified couple stress theories. Afterwards, three important functions of the microbeams which are used as microsensors, sensitivity, quality factor, and maximum stress are defined. In the subsequent stage, two and three objective optimizations are carried out by using the genetic algorithm. At the two-objective optimization, sensitivity and quality factor are selected as objective functions. At the three objective optimizations, the maximum stress adds to the objective functions. The geometric parameters are design variables and there are some constraints and limits for those. The results are presented based on the classical and non-classical theory and optimal points are obtained for each optimization by using MATLAB.

Keywords: Multi-objective optimization, Microsensor, Microbeam, Sensitivity, Quality factor

1 Introduction

Many microelectromechanical systems (MEMS) are utilized for distinct applications such as energy harvesting and sensing [1, 2]. Some of the microsensors are used for the measurement of the special physical parameters. Nazemi, Joseph, Park and Emadi [3] reviewed Advanced micro and nano-gas sensor. Tian, Zhao, Jiang and Hu [4] designed and analyzed beam-membraned structure sensor for micro-pressure measurement. Bouchaala, Nayfeh, Jaber and Younis [5] studied mass and position determination in MEMS mass sensor. Also, some of these studies were about microsensors which are used for the virus identification. Kurmendra and Kumar [6] reviewed MEMS based cantilevers biosensors for cancer detection. Kim, Jeon, Cho,

[*] M.Sc., Faculty of Mechanical and Energy Engineering, Shahid Beheshti University, Tehran, Iran, m.davoodiyekta@mail.sbu.ac.ir, Tel: +98 9027961369
[†] Corresponding Author, Assistant Professor, Faculty of Mechanical and Energy Engineering, Shahid Beheshti University, Tehran, Iran, a_rahi@sbu.ac.ir, Tel: +98 9372737526

Received: 2022/02/15, Revised: 2022-11-24, Accepted: 2022/12/22

Cheong, Moon and Go [7] presented a Highly sensitive microcantilever biosensors for detection of human papilloma virus. Kabir, Merati and Abdekhodaei designed an effective piezoelectric microcantilever biosensor for rapid detection of COVID-19.

In the other hand, to investigate the operation of these systems according to the dynamic of them, it is necessary to implement a physical model and derive governing equations. Microbeams as a microsensor are one of the most general models of MEMS [2]. Park and Gao [8] presented Bernoulli–Euler beam model based on a modified couple stress theory for microbeams. The new model contained material length scale parameters and could investigate the effects of the size. Their model predicted bending rigidity larger than the classical model. Liang, Ke, Wang, Yang, and Kitipornchai [9] investigated the flexural vibration of an atomic force microscope cantilever based on the modified couple stress theory. They implemented a Timoshenko model and derived equations of motion by using Hamilton's principle. Results show that when the value of the material length scale parameter is like the value of the thickness, the size has a significant effect on the natural frequency.

Dai, K. Wang, and L. Wang, [10] developed a new nonlinear model for cantilever microbeams based on the modified couple stress theory. The equation of motion is valid for large deformation. The numerical results were presented in the form of frequency-response curves. Thai, Vo, Nguyen and Kim [11] presented a review of the continuum models to investigate the size effect in the analysis of beams and plates. Ghayesh, Farokhi, and Gholipour [12] studied the vibration of the geometrically imperfect three-layered shear deformable microbeams. The effects of some parameters such as material length scale and material friction were investigated. Ding, Xu, Zheng, and Li [13] investigated the size-dependent nonlinear dynamic of the microbeams based on the modified couple stress theory. The effect of the thickness, width, and gap between electrodes on the frequency response and picking amplitude were investigated. Rahi [14] studied the lateral vibration of micro-overhung rotor-disk subjected to an axial load. The governing equations were derived based on the modified strain gradient theory and Hamilton's principle. The effects of the parameters such as material length scale and rotational speed on the natural frequency and instability speed were presented.

Karamanli and Aydogdu [15] analyzed size-dependent rotating laminated and sandwich microbeams. They studied the eigenfrequencies of these microbeams with various boundary conditions. Also, various values of the different parameters such as aspect ratio and fiber orientation angles are employed to complete the study. Andre Gusso [16] investigated nonlinear damping in microbeams which is resulting from surface energy loss. They modeled the resonator as a clamped-clamped microbeam. Jahangiri, Asghari, and Bagheri [17] investigated torsional vibration in the micro-rotors based on the modified couple stress theory. Some parametric studies were presented to investigate the effects of parameters such as material length scale on the natural frequency and super-harmonic resonant amplitude.

Gan and Wang [18] presented a topology optimization design considering the size effect and based on the modified couple stress theory. They utilized a bi-directional evolutionary structural optimization method. Pan, Li, M. Wang, and L. Wang [19] presented elastothermodynamic damping modeling of a three-layer Kirchhoff–Love microplate considering three-dimensional heat conduction. They used typical boundary conditions such as Clamped-Clamped-Clamped-Clamped to model the microplate. Loghman, Bakhtiari-Nejad, Kamali E., Abbaszadeh, and Amabili [20] investigated the nonlinear vibration of fractional viscoelastic microbeams. The modified couple stress theory is used to consider the size effects. The effects of the order of the fractional derivative, viscoelastic model, and micro-scale had been studied numerically. Rahi [21] analyzed the vibration of the multi-layer micro beams based on the modified couple stress theory and obtained the first three natural frequencies.

Eftekhari and Toghraei [22] investigated the dynamic and vibration of a cantilever sandwich microbeam integrated with piezoelectric layers. The strain gradient theory and Hamilton's

principle were implemented to derive equations of motion. The effects of the various material length scale, geometry, and surface parameters had been studied.
There is a lack of optimization of the practical microbeams in the literature. In other words, there is not a study about the optimal microbeam which has the best performance according to the important parameters of the sensing. In this paper two and three objective optimizations of a multi-layer microbeam that is used as a microsensor is presented. Sensitivity, quality factor, and maximum stress are the target functions. It is also worth noting that geometric parameters are design variables and the optimization is carried out under the guidance of the genetic algorithm. Optimizations are presented based on classical and non-classical (modified couple stress) theories.

2 Modeling

There is a microbeam that has 2 layers. One layer is silicon and the other one is quartz as a piezoelectric. The boundary conditions are simply supported. It is assumed that there is no slipping between layers. For simplification, nonlinearity effects are neglected. As it has been shown in Figure (1), the thickness of the layers are h_i and the length is L. Also, the width of the microbeam is b.
There are some external particles in many sensing systems that sit on the sensor and the mass of the system undergoes a change. This change leads to frequency change. In this paper, it is assumed that external particles are viruses and the sensor is applied to detect viruses.
The microbeam has a transverse vibration and the displacement field is defined as follows:

$$w(x,t) = X(x)T(t) \tag{1}$$

where

$$T(t) = e^{i\omega_0 t} \tag{2}$$

$$X = X_{max}\left(\sin\left(\frac{\pi x}{L}\right)\right) \tag{3}$$

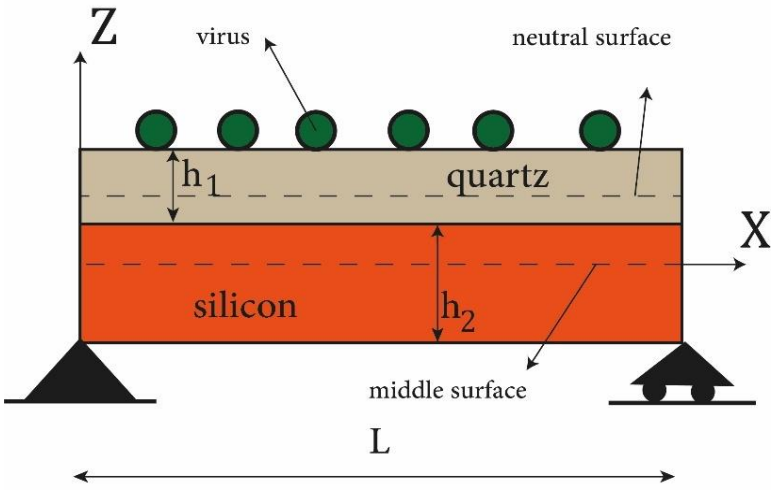

Figure 1 2-layer simply supported microbeam

To calculate the first natural frequency ω_0, Rayleigh's method is used. The kinetic, potential energy are calculated based on Rahi's research [21]. Also, in this paper, the first natural frequency is calculated as:

$$\omega_0 = \left(\frac{N\left(\frac{\pi^4}{2L^3}\right)}{M(0.486)L + G\left(\frac{\pi^2}{2L}\right)} \right)^{\frac{1}{2}} \tag{4}$$

where

$$N = \left\{ \sum_{i=1}^{n} E_i \tilde{I}_i + \frac{6E_i \bar{I}_i}{(1+\nu_i)} \left(\frac{l_i}{h_i}\right)^2 \right\}$$

$$M = \left(\sum_{i=1}^{n} \rho_i A_i \right) \tag{5}$$

$$G = \left(\sum_{i=1}^{n} \rho_i \tilde{I}_i \right)$$

In these formulas ρ_i is the density of each layer, A_i is the area of each layer. h_i is the thickness of each layer. E_i , ν_i , l_i are Young's module, Poisson's coefficient, and material length scale parameter, respectively. Also, $\tilde{I}_i$ is the moment of inertia and is the function of dimensions.
The function X which is defined in Equation (3) is opted based on the boundary conditions. This microbeam is simply supported therefore displacement on the two end of the microbeam is zero. If set X=0 or L, the value of the function will be zero and geometrical boundary conditions satisfy.
To obtain X_{max}, the system is modeled as a simple mass-spring system and X_{max} is obtained as:

$$X_{max} = \frac{F}{k} \tag{6}$$

where F is the weight of the virus particles and is defined as:

$$F = (\Delta m g) \tag{7}$$

where Δm is the external mass.
If the area of the particles, or the area of the contact surface, and the area of the microbeam, or the top surface of the microbeam, are A_p and A_b respectively so:

$$\Delta m = \left(\frac{A_b}{A_p}\right) m_p = \left(\frac{bL}{A_p}\right) m_p \tag{8}$$

where m_p is the mass of a single particle.

Also, k is the stiffness of the system and based on equation (4) is calculated as:

$$k = N\left(\frac{\pi^4}{2L^3}\right) \tag{9}$$

There are some functions which are of paramount importance for sensors such as sensitivity and quality factor that describe the accuracy and quality of the measurement. Sensitivity is the relation between mass and frequency changes. If the sensitivity is high, it means a minor change in the mass of the system could be detected. The sensitivity is defined as [2]:

$$S = \frac{\Delta f}{\Delta m} = -\frac{2{f_0}^2}{A\sqrt{\rho\mu}} \tag{10}$$

where A is the active area of the piezoelectric and ρ, μ are the density and the shear module of the piezoelectric respectively. Also, f_0 is calculated as:

$$f_0 = \frac{\omega_0}{2\pi} \tag{11}$$

The quality factor is the function that shows the quality of the measurement. In other words, when the quality factor is high, the quality of the measurement is better. This function is defined as [23]:

$$Q^{-1} = \frac{E\alpha^2 T_o}{C_p}\left(\frac{6}{\xi^2} - \frac{6}{\xi^3}\frac{\sinh(\xi)+\sin(\xi)}{\cosh(\xi)+\cos(\xi)}\right) \tag{12}$$

where E is Young's module, C_p, α, $and\ T_o$ are the heat capacity, the thermal expansion coefficient, and the surrounding temperature respectively and

$$\xi = b\sqrt{\frac{\omega_0}{2\chi}} \tag{13}$$

where

$$\chi = \frac{H}{\rho C_p} \tag{14}$$

where H is the conductivity and ρ is the density.
The model of the microbeam is two layers so in Equations (12-14) values are approximated by the mean values of the layers. For example:

$$E_e = \frac{E_1 h_1 + E_2 h_2}{h_1 + h_2} \tag{15}$$

Another imperative function is the maximum stress. When the maximum stress increases, the safety of the system would decrease because the probability of failure increases. The maximum stress is defined as [24]:

$$\sigma_{max} = (Ez)_{max}(\frac{\partial^2 X}{\partial x^2})_{max} \tag{16}$$

Considering the two layers of the micro-beam and the equations (3, 6-9), the above equations can be rewritten as follows:

$$\sigma_{max} = C\ (E_i h_i)_{max} \frac{(bL)}{N\left(\frac{\pi^4}{2L^3}\right)} \left(\frac{\pi}{L}\right)^2 \tag{17}$$

or

$$\sigma_{max} = C\ \sigma^* \tag{18}$$

where C is:

$$C = \frac{g\rho_p}{A_p} \tag{19}$$

So far, the most important functions pertaining to microbeams used as sensors have been introduced. In the subsequent stage, the optimization of this type of microbeam will be discussed. First, by considering the sensitivity and quality factor as objective functions, two-objective optimization is performed. Then, by adding the maximum stress to the objective functions, a three-objective optimization will take place.

3 Two-objective optimization

In the first step, two objective optimization Nonwas done by using a genetic algorithm. The sensitivity and quality factor are two objective functions including dimensions. These functions are defined as:

$$S = f_1(h_1, h_2, b, L) \tag{20}$$

$$-Q = f_2(h_1, h_2, b, L) \tag{21}$$

As it has been shown in Equation (21), the negative value of the quality factor is one of the objective functions. This has happened due to the fact that the genetic algorithm discovers the minimum values of the functions but as it is mentioned before, to enhance quality, the quality factor must be improved and the maximum value must be figured out. Also according to Equations (20,21), the design variables are h_1, h_2, b, L. The constraints of design are defined as:

$$h_1 + h_2 \leq 0.1L \tag{22}$$

$$2(h_1 + h_2) \leq b \tag{23}$$

$$L \geq 3b \tag{24}$$

The coefficients that appears in Equations (22-24) are arbitrary but these constraints should be applied to prevent finding the points that are not authentic based on the geometrical assumptions. If they are not applied, the points would be found which have a bigger width than the length, for example. In addition, the lower and upper bound of design variables and the properties of the layer's material are pinpointed in Table (1,2), respectively.
The MATLAB software is used for optimization and 18 optimal points are found based on both classical and non-classical theories. Previous equations were calculated based on classical theory. If l_i in Equation (5) is set to zero, the results will be obtained based on the non-classical theory.
The values of the objective functions with the values of the design variables in the optimal points are shown in tables (3,4). Table (3) illustrates the results that are obtained based on the classical theory and table (4) shows the non-classical one. Among all the design variables, the thickness of the piezoelectric is the least important because the changes in this variable value are less than others and are about 1%. Technically all the optimal points have approximately same thickness.

Table 1 The lower and upper bounds

Variable	Lower bound(10^{-6})	Upper bound(10^{-6})
$x(1)$	10	100
$x(2)$	10	100
$x(3)$	40	300
$x(4)$	200	1000

Table 2 Properties of the materials [25]

Property/material	Unit	SiO_2(quartz)	Si
E	Gpa	72.52	170
N	-	0.166	0.22
M	Gpa	30.97	69.67
P	kg/m^3	2650	2233
l	μm	2.4	1
C	J/kg K	700	812.33
H	W/m K	1.3	156
A	10^{-6}/K	12.3	0.262

Table 3 Description of the optimal point based on the non-classical theory (Two-objective optimization)

Design variables				Objective functions	
$h_1(\mu m)$	$h_2(\mu m)$	$b(\mu m)$	$L(\mu m)$	S	-Q
10	10.00001	40.00007	200.0001	-3.88E+19	-2036797
10.01901	11.35231	43.5109	720.0225	-2.46E+17	-7.8E+07
10.00691	10.01056	40.06431	635.5686	-3.83E+17	-7E+07
10.00509	11.17875	42.48153	611.7689	-4.76E+17	-3.8E+07
10.00468	11.17899	42.48131	611.7688	-4.76E+17	-2.6E+07
10.01219	10.35013	40.75713	639.182	-3.82E+17	-7.2E+07
10.01901	11.35231	43.5109	720.0225	-2.46E+17	-7.8E+07
10.00159	10.07924	40.18488	218.64	-2.73E+19	-2427589
10	10.00001	40.00007	200.0001	-3.88E+19	-2036797
10.00173	10.00276	40.01614	308.289	-6.91E+18	-4764419
10.00172	10.01772	40.11404	269.3141	-1.18E+19	-3703092
10.00097	10.04725	40.46914	227.1184	-2.32E+19	-2553050
10.00439	10.82472	41.88108	606.0759	-4.83E+17	-1.9E+07
10.00142	10.25892	41.16421	239.037	-1.90E+19	-2798615
10.00176	10.35051	40.90174	212.8613	-3.07E+19	-2248415
10.00087	10.02506	40.05425	231.4272	-2.17E+19	-2734157
10.00183	10.03308	40.11689	209.2467	-3.24E+19	-2227478
10.00149	10.26653	41.57221	245.8099	-1.69E+19	-2884708

Table 4 Description of the optimal point based on the classical theory (Two-objective optimization)

Design variables				Objective functions	
$h_1(\mu m)$	$h_2(\mu m)$	$b(\mu m)$	$L(\mu m)$	S	-Q
10	10.00001	40.00007	200.0082	-3.88E+19	-2044203.6
10.00001	10.00001	40.00013	212.5398	-3.04E+19	-2313396.7
10.00001	10.00001	40.00004	289.8286	-8.84E+18	-4391840.4
10.00001	10.00001	40.00007	200.0002	-3.88E+19	-2044202
10.03435	10.09113	40.54201	757.0462	-1.90E+17	#NAME?
10.16005	10.26292	40.89201	727.7444	-2.24E+17	-70835904
10.10925	11.79615	44.3718	622.6984	-4.51E+17	-26636923
10.04767	11.66927	44.15664	375.9384	-3.36E+18	-6773119.1
10.13482	10.76489	41.83812	663.0096	-3.35E+17	-36892767
10.06463	11.24589	42.96567	487.5611	-1.17E+18	-11843581
10.08699	11.35119	43.07463	532.2448	-8.32E+17	-17211213
10.12257	11.19898	42.90853	599.8223	-5.10E+17	-19084673
10.12367	11.97743	44.21448	646.7196	-3.96E+17	-26961257
10.01838	10.13986	40.55102	452.5007	-1.49E+18	-10135445
10.07844	10.60038	41.69286	501.764	-1.01E+18	-12198685
10.04287	10.12313	40.77347	669.8415	-3.09E+17	-70716326
10.00001	10.00001	40.00004	270.3355	-1.17E+19	-3698391.8
10.00415	10.0014	40.12365	222.9417	-2.51E+19	-2509075.9

The most important variable is the length which has about 375% changes. It shows that the length has significant effects on the values of the objective functions and should be taken into consideration far more than other variables.
The pareto front of the objective functions in optimal points is shown in Figures (2,3) based on both theories. It is obvious that the values are approximately the same based on both theories. Also, it can be inferred from the figures that the functions have contradictory behavior because the ideal points which are located almost on the bisector of the axes are very far from the origin. To find ideal points, first, the values should be normalized by using Equation (25):

$$\bar{\Psi} = \frac{\Psi_i(j) - \max[\Psi_i(j)]}{\min\ [\Psi_i(j)] - \max[\Psi_i(j)]}\ , \quad \bar{\Psi} = \bar{S}\ , \bar{Q}$$
$$\bar{\Psi} = \frac{\Psi_i(j) - min\ [\Psi_i(j)]}{\max\ [\Psi_i(j)] - min\ [\Psi_i(j)]}\ , \quad \bar{\Psi} = \overline{\sigma^*} \tag{25}$$

The ideal points are the farthest points and between these minimum values have the largest values in other words to find the best answers Equation (26) is used.

$$\Upsilon = Max(-\bar{S} - \bar{Q}) \tag{26}$$

The values of ideal points are described in Table (5).
The microbeam which is selected based on the classical theory is bigger than that of selected based on the non-classical theory. The thickness of the silicon is approximately equal to the lower bound and both functions are so far from the maximum.

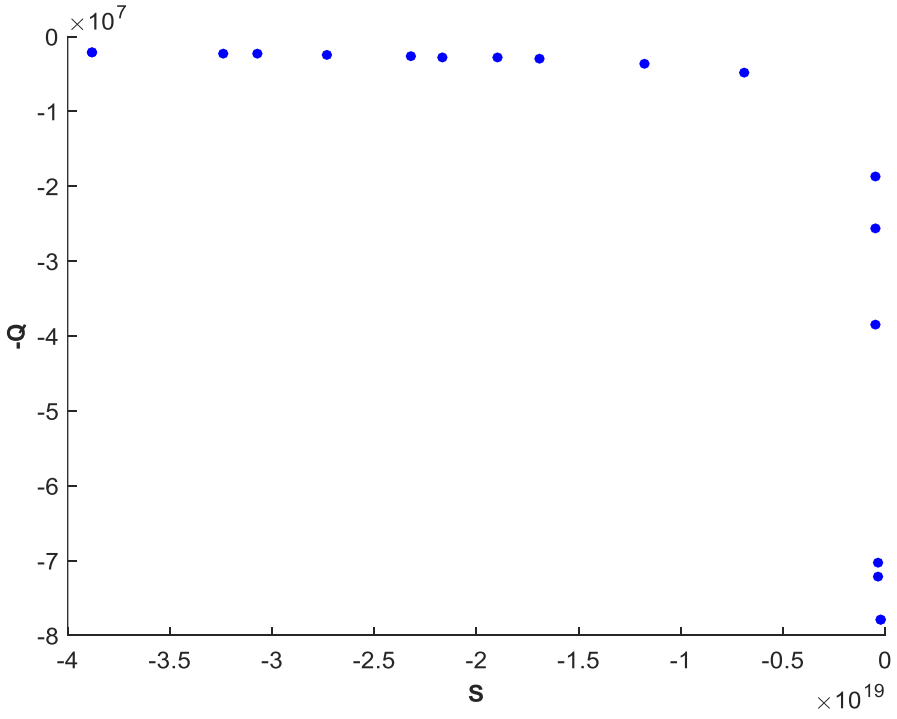

Figure 2 The pareto front of the objective functions in optimal points, based on the non-classical theory

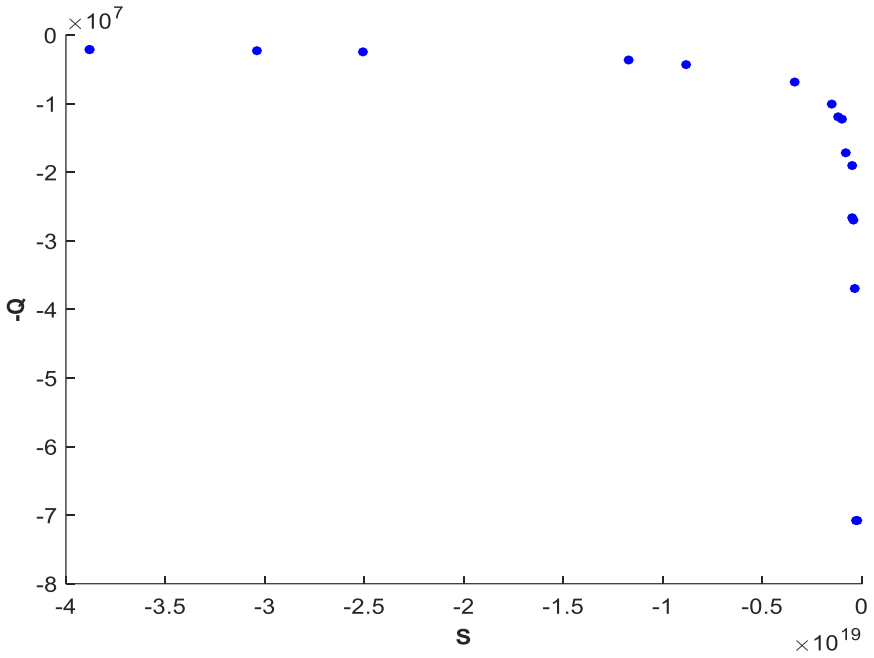

Figure 3 The pareto front of the objective functions in optimal points, based on classical theory.

Table 5 The ideal points in two-objective optimization

Theory	h_1 (μm)	h_2 (μm)	b (μm)	L (μm)	S	$-Q$	$\sum \bar{\Psi}$
Non-classical	10.00	10.00	40.01	308.28	-6.91E+18	-4764419	-0.208
Classical	10.047	11.66	44.15	375.93	-3.36E+18	-6773119.1	-0.150

4 Three-objective optimization

In this section, one more function adds to objective functions and three-objective optimization is done. As well as mentioned before, maximum stress is the critical function which the safety of the system is related to. Therefore, to improve the system, the maximum stress should be decreased. The third objective function is defined as:

$$\sigma^* = f_3(h_1, h_2, b, L) \tag{27}$$

According to Equation (18), σ^* is the changeable part of the maximum stress and is selected as an objective function. The minimum value of the σ^* is obtained at a point that has the minimum value of maximum σ. All of the constraints, boundary conditions, and bounds are the same in comparison with previous section.

The results based on the non-classical and classical theories are presented in Tables (6,7). Unlike the previous, thickness of the piezoelectric is very important and also it has a significant change, more than 100%. This difference is due to the third objective function. To decrease maximum stress, the thickness of the piezoelectric should be increased.

As Same as two objective optimizations the length of the microbeam is the most important variable and has more than 200% changes. Approximately at all the points that have high sensitivity and low stress, the quality factor is low undesirable. When the dimensions are large, sensitivity is low however, the quality factor is high.

Table 6 Description of the optimal point based on the non-classical theory (Three-objective optimization)

Design variables				Objective functions		
$h_1(\mu m)$	$h_2(\mu m)$	$b(\mu m)$	$L(\mu m)$	S	-Q	σ^*
10.00001	10.00001	40.00007	200.0002	-5.37E+18	-5405342	193.9582
13.03221	10.69175	50.92351	564.0295	-7.14E+16	-6.1E+07	991.4873
10.93447	14.0286	50.67345	484.3055	-1.80E+17	-4.3E+07	811.2724
10.75598	14.19547	50.27158	521.3468	-1.38E+17	-4.5E+07	950.8082
10.31625	13.15566	47.21637	460.1513	-2.22E+17	-4.3E+07	826.5051
20.59833	10.00008	64.57942	305.9847	-6.66E+17	-1375276	127.438
10.00001	10.00001	40.00007	200.0002	-5.37E+18	-5511329	193.9582
20.17613	10.00047	63.60115	301.7665	-7.11E+17	-1438157	129.1941
10.52122	15.08772	51.55225	623.1986	-7.16E+16	-4.8E+07	1327.079
17.73594	10.00001	57.9402	277.3601	-1.06E+18	-1839345	140.4387
12.1846	11.64869	48.44027	353.4557	-5.30E+17	-1E+07	417.4656
15.22577	10.07447	53.85419	266.6986	-1.30E+18	-2590799	172.3256
10.00001	10.00001	40.00007	200.0002	-5.37E+18	-5621555	193.9582
20.59805	10.00031	64.57948	305.9845	-6.66E+17	-1380589	127.4413
16.04507	10.00003	54.01909	260.4517	-1.43E+18	-2204859	149.534
11.59445	11.20332	46.16022	312.0009	-8.80E+17	-9119975	357.356
10.02362	11.50198	43.51302	250.0708	-2.36E+18	-8077744	278.327
17.73594	10.00001	57.9402	277.3601	-1.06E+18	-1839345	140.4387

Table 7 Description of the optimal point based on the classical theory (Three-objective optimization)

Design variables				Objective functions		
$h_1(\mu m)$	$h_2(\mu m)$	$b(\mu m)$	$L(\mu m)$	S	-Q	σ^*
10.00001	10.00001	40.00004	200.0002	-5.37E+18	-5405342	193.9583
19.39867	10.00001	59.87561	293.9867	-8.29E+17	-1648422	132.5585
10.06362	13.42987	47.05403	464.1174	-2.22E+17	-9E+07	853.3362
10.03196	10.3022	40.83423	361.8783	-5.08E+17	-3.6E+07	621.9785
10.06865	13.54808	47.45675	499.2988	-1.66E+17	-9.1E+07	980.1989
10.04173	10.64251	42.53186	436.3329	-2.39E+17	-7.4E+07	886.5531
10.0494	12.56905	45.50196	421.1854	-3.12E+17	-4.2E+07	740.2274
10.06363	13.42994	47.05354	464.1174	-2.22E+17	-4.5E+07	853.3316
10.00548	10.09296	40.49045	214.9609	-4.02E+18	-6289638	222.7829
10.02145	10.03341	40.32878	237.8772	-2.67E+18	-8274834	273.0353
10.06684	13.55043	47.45416	499.2983	-1.67E+17	-9.1E+07	980.2743
10.03611	11.87771	44.02136	361.663	-5.55E+17	-2E+07	568.912
19.39867	10.00001	59.87457	293.9867	-8.29E+17	-1626636	132.5585
10.03555	10.34632	41.06736	231.2434	-3.04E+18	-7025317	253.2432
10.02098	10.12818	40.44247	252.5567	-2.12E+18	-8858499	306.2567
10.04369	11.02939	43.06111	444.4524	-2.29E+17	-7.6E+07	900.277
10.06682	11.56334	43.86083	293.0747	-1.25E+18	-1.1E+07	378.7585
10.01345	10.02569	40.29685	225.3182	-3.32E+18	-6862215	245.354

Figures (4,5) show the behavior of the objective functions at optimal points. Results are presented based on the classical and non-classical theories and have many similarities. To find the best point among these points, a similar method to the previous section is used. Functions are normalized by using Equations (25,28). Equation (28) is:

$$\bar{\Psi} = \frac{\Psi_i(j) - min\,[\Psi_i(j)]}{\max\,[\Psi_i(j)] - min\,[\Psi_i(j)]}\ , \quad \bar{\Psi} = \overline{\sigma^*} \tag{28}$$

and the ideal points are obtained by using Equation (29):

$$\Upsilon = Max(-\bar{S} - \bar{Q} + \overline{\sigma^*}) \tag{29}$$

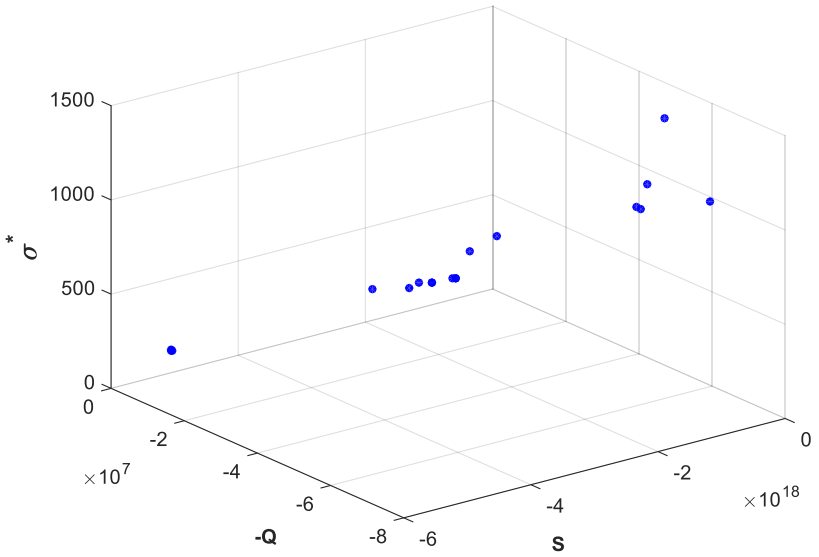

Figure 4 The behavior of the objective functions at optimal points based on non-classical theory

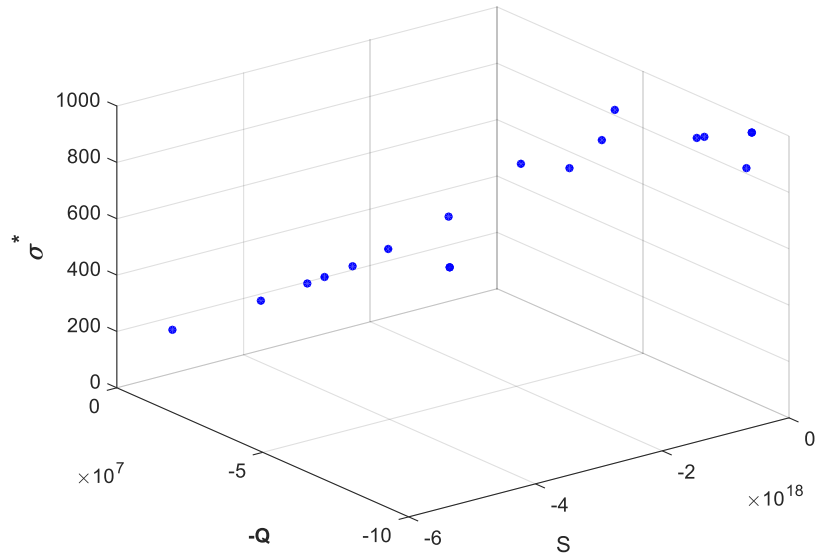

Figure 5 The behavior of the objective functions at optimal points based on non-classical theory

Table 8 The ideal points in three-objective optimization

Theory	h_1 (μm)	h_2 (μm)	b (μm)	L (μm)	S	$-Q$	σ^*	$\sum \bar{\Psi}$
Non-classical	10.52	15.08	51.55	623.19	-7.16E+16	-4.8E+07	1327.079	0.207
classical	10.06	13.42	47.05	464.11	-2.22E+17	-4.5E+07	853.3316	0.352

The ideal points are presented in Table (8).
Compared to the two-objective optimization, the dimensions, especially the length, increase. Unlike the previous section, the ideal microbeam based on the non-classical theory is bigger than the classical one. Conversely, as well as the prior section, the value of the objective functions compared to their maximum are very low.
The magnitude of the sensitivity compared to the two-objective optimization decreased but that of the quality factor did not have significant changes. In other words, when the maximum stress is added to the objective functions, the characteristics of optimal points change in a way that doesn't have effects on the quality factor but changes sensitivity. It can be inferred that sensitivity and stress are correlated but not to the quality factor.

5 Conclusion

Multi-objective optimization of the simply supported microbeam used as a sensor was carried out in this research. The model had two-layer and transverse vibration. In the first step two-objective optimization was done while the sensitivity and quality factors were selected as objective functions. In the second step, the maximum stress was added to the objective functions. The design variables were the dimensions of the microbeam and optimization was done by MATLAB software. The results mentioned below were obtained:

- The length is the most important variable.
- The sensitivity and the maximum stress are correlated but with the quality factor.
- In two-objective optimization, the changes in the piezoelectric layer are very minor but when the maximum stress is one of the objective functions, it increased significantly.
- The sensitivity is high when the dimensions are small.
- The quality factor is high when the dimensions are large.

Compliance with Ethical Standards

The authors declare that they have no conflict of interest.

References

[1] M. T. Todaro et al., "Piezoelectric MEMS Vibrational Energy Harvesters: Advances and Outlook," *Microelectronic Engineering*, vol. 183, pp. 23-36, 2017, https://doi.org/10.1016/j.mee.2017.10.005.

[2] F. Narita et al., "A Rview of Piezoelectric and Magnetostrictive Biosensor Materials for Detection of COVID-19 and Other Viruses," *Advanced Materials*, vol. 33, no. 1, p. 2005448, 2021, https://doi.org/10.1002/adma.202005448.

[3] H. Nazemi et al., "Advanced Micro-and nano-gas Sensor Technology: A Review," *Sensors*, vol. 19, no. 6, p. 1285, 2019, https://doi.org/10.3390/s19061285.

[4] B. Tian et al., "The Design and Analysis of Beam-membrane Structure Sensors for Micro-pressure Measurement," *Review of Scientific Instruments*, vol. 83, no. 4, 2012, https://doi.org/10.1063/1.3702809.

[5] A. Bouchaala et al, "Mass and Position Determination in MEMS Mass Sensors: A Theoretical and an Experimental Investigation," *Journal of Micromechanics and Microengineering*, vol. 26, no. 10, p. 105009, 2016, 10.1088/0960-1317/26/10/105009.

[6] Kurmendra and R. Kumar, "MEMS Based Cantilever Biosensors for Cancer Detection Using Potential Bio-markers Present in VOCs: A Survey," *Microsystem Technologies*, vol. 25, no. 9, pp. 3253-3267, 2019, https://doi.org/10.1007/s00542-019-04326-1.

[7] H. H. Kim et al., "Highly Sensitive Microcantilever Biosensors with Enhanced Sensitivity for Detection of Human Papilloma Virus Infection," *Sensors and Actuators B: Chemical*, vol. 221, pp. 1372-1383, 2015, https://doi.org/10.1016/j.snb.2015.08.014.

[8] S. Park and X. Gao, "Bernoulli–Euler Beam Model Based on a Modified Couple Stress Theory," *Journal of Micromechanics and Microengineering*, vol. 16, no. 11, p. 2355, 2006, 10.1088/0960-1317/16/11/015.

[9] L.-N. Liang et al, "Flexural Vibration of an Atomic Force Microscope Cantilever Based on Modified Couple Stress Theory," *International Journal of Structural Stability and Dynamics*, vol. 15, no. 07, p. 1540025, 2015, https://doi.org/10.1142/S0219455415400258.

[10] H. Dai, Y. Wang and L. Wang, "Nonlinear Dynamics of Cantilevered Microbeams Based on Modified Couple Stress Theory," *International Journal of Engineering Science*, vol. 94, pp. 103-112, 2015, https://doi.org/10.1016/j.ijengsci.2015.05.007.

[11] H.-T. Thai et al., "A Review of Continuum Mechanics Models for Size-dependent Analysis of Beams and Plates," *Composite Structures*, vol. 177, pp. 196-219, 2017, https://doi.org/10.1016/j.compstruct.2017.06.040.

[12] M. H. Ghayesh, H. Farokhi, and A. Gholipour, "Vibration Analysis of Geometrically Imperfect Three-layered Shear-deformable Microbeams," *International Journal of Mechanical Sciences*, vol. 122, pp. 370-383, 2017, https://doi.org/10.1016/j.ijmecsci.2017.01.001.

[13] N. Ding et al, "Size-dependent Nonlinear Dynamics of a Microbeam Based on the Modified Couple Stress Theory," *Acta Mechanica*, vol. 228, pp. 3561-3579, 2017, https://doi.org/10.1007/s00707-017-1895-3.

[14] A. Rahi, "Lateral Vibration of a Micro Overhung Rotor-disk Subjected to an Axial Load Based on the Modified Strain Gradient Theory," *International Journal of Structural Stability and Dynamics*, vol. 18, no. 09, p. 1850114, 2018, https://doi.org/10.1142/S0219455418501146.

[15] A. Karamanli and M. Aydogdu, "On the Vibration of Size Dependent Rotating Laminated Composite and Sandwich Microbeams via a Transverse Shear-normal Deformation Theory," *Composite Structures*, vol. 216, pp. 290-300, 2019, https://doi.org/10.1016/j.compstruct.2019.02.044.

[16] A. Gusso, "Nonlinear Damping in Suspended Beam Micro-and Nanoresonators Due to Surface Loss," *Journal of Sound and Vibration*, vol. 467, p. 115067, 2020, https://doi.org/10.1016/j.jsv.2019.115067.

[17] M. Jahangiri, M. Asghari, and E. Bagheri, "Torsional Vibration Induced by Gyroscopic Effect in the Modified Couple Stress Based Micro-rotors," *European Journal of Mechanics-A/Solids*, vol. 81, p. 103907, 2020, https://doi.org/10.1016/j.euromechsol.2019.103907.

[18] N. Gan and Q. Wang, "Topology Optimization Design Related to Size Effect Using the Modified Couple Stress Theory," *Engineering Optimization*, vol. 55, no. 1, pp. 158-176, 2023, https://doi.org/10.1080/0305215X.2021.1990911.

[19] W. Pan et al, "Elastothermodynamic Damping Modeling of Three-layer Kirchhoff–Love Microplate Considering Three-dimensional Heat Conduction," *Applied Mathematical Modelling*, vol. 89, pp. 1912-1931, 2021, https://doi.org/10.1016/j.apm.2020.09.005.

[20] E. Loghman et al., "Nonlinear Vibration of Fractional Viscoelastic Micro-beams," *International Journal of Non-Linear Mechanics*, vol. 137, p. 103811, 2021, https://doi.org/10.1016/j.ijnonlinmec.2021.103811.

[21] A. Rahi, "Vibration Analysis of Multiple-layer Microbeams Based on the Modified Couple Stress Theory: Analytical Approach," *Archive of Applied Mechanics*, vol. 91, no. 1, pp. 23-32, 2021, http://dx.doi.org/10.1007/s00419-020-01795-z.

[22] S. A. Eftekhari and D. Toghraie, "Vibration and Dynamic Analysis of a Cantilever Sandwich Microbeam Integrated with Piezoelectric Layers Based on Strain Gradient Theory and Surface Effects," *Applied Mathematics and Computation*, vol. 419, p. 126867, 2022, https://doi.org/10.1016/j.amc.2021.126867.

[23] R. Lifshitz and M. L. Roukes, "Thermoelastic Damping in Micro-and Nanomechanical Systems," *Physical Review B*, vol. 61, no. 8, p. 5600, 2000, https://doi.org/10.1103/PhysRevB.61.5600.

[24] E. Taati and N. Sina, "Multi-objective Optimization of Functionally Graded Materials, Thickness and Aspect Ratio in Micro-beams Embedded in an Elastic Medium," *Structural and Multidisciplinary Optimization*, vol. 58, pp. 265-285, 2018, https://doi.org/10.1007/s00158-017-1895-x.

[25] I. V. Semiconductor, "Basic Mechanical and Thermal Properties of Silicon," *Growth (Lakeland)*, vol. 22401, no. 540, pp. 1-4, 2000. 22401(540).